Influence of Rashba spin-orbit coupling on the Kondo effect

Arturo Wong, Sergio E. Ulloa, Nancy Sandler, and Kevin Ingersent

Influence of Rashba spin-orbit coupling on the Kondo effect

Arturo Wong,[1, *] Sergio E. Ulloa,[2] Nancy Sandler,[2] and Kevin Ingersent[1]

[1]*Department of Physics, University of Florida, P.O. Box 118440, Gainesville, Florida 32611-8440, USA*
[2]*Department of Physics and Astronomy, Nanoscale and Quantum
Phenomena Institute, Ohio University, Athens, Ohio 45701, USA*

(Dated: February 1, 2016)

An Anderson model for a magnetic impurity in a two-dimensional electron gas with bulk Rashba spin-orbit interaction is solved using the numerical renormalization group under two different experimental scenarios. For a fixed Fermi energy, the Kondo temperature T_K varies weakly with Rashba coupling α, as reported previously. If instead the band filling is low and held constant, increasing α can drive the system into a helical regime with exponential enhancement of T_K. Under either scenario, thermodynamic properties at low temperatures T exhibit the same dependences on T/T_K as are found for $\alpha = 0$. Unlike the conventional Kondo effect, however, the impurity exhibits static spin correlations with conduction electrons of nonzero orbital angular momentum about the impurity site. We also consider a magnetic field that Zeeman splits the conduction band but not the impurity level, an effective picture that arises under a proposed route to access the helical regime in a driven system. The impurity contribution to the system's ground-state angular momentum is found to be a universal function of the ratio of the Zeeman energy to a temperature scale that is not T_K (as would be the case in a magnetic field that couples directly to the impurity spin), but rather is proportional to T_K divided by the impurity hybridization width. This universal scaling is explained via a perturbative treatment of field-induced changes in the electronic density of states.

I. INTRODUCTION

The field of spintronics has primarily been driven by the idea of manipulating spin states to create new, spin-based electronic devices[1,2]. Rashba spin-orbit (SO) coupling[3] has been proposed as a mechanism for spin-control, not only because of the possibility of its external manipulation, but also because it is the physical origin of spin-dependent phenomena such anisotropic magnetoresistance[4] and the spin-Hall effect[5]. Interest in SO interactions has also been motivated by the recent discovery of large Rashba spin-splittings in Bi_2Se_3 topological insulators[6,7], where the Rashba parameter can be an order of magnitude higher than in standard III-V semiconductors.

The study of Kondo correlations in the presence of SO interactions can be traced back more than 40 years to experiments that seemed to demonstrate suppression of the Kondo effect by Pt impurities[8]. However, early theoretical studies of Anderson and Kondo models including SO scattering from heavy nonmagnetic impurities reached opposing conclusions as to whether SO interactions cut off the Kondo $\ln(T/T_K)$ term in the resistivity[9,10]. Subsequent magnetoresistance measurements were interpreted as providing evidence for coexistence of SO scattering and the Kondo effect[11]. A similar conclusion was reached on the basis of time-reversal symmetry[12], although this assertion has recently been challenged[13].

In recent years, several theoretical works have investigated the effect of SO interaction of the Rashba type on the Kondo temperature T_K. An analysis of the Kondo model for a magnetic impurity in an otherwise clean two-dimensional electron gas (2DEG) concluded that T_K remains essentially unchanged by Rashba coupling[14]. A numerical renormalization-group (NRG) study of an Anderson model describing the same physical situation similarly predicted weak enhancement or depression of T_K, depending on the energy of the impurity level relative to the Fermi energy[15]. A variational treatment of the Kondo problem for arbitrary band dispersion and a general SO coupling also found no significant change of T_K, although it was claimed that the impurity is only partially screened[16]. By contrast, a mapping via a generalized Schrieffer-Wolff transformation[17] of an Anderson impurity in a two-dimensional host to an effective Kondo model led to the prediction[18] of an exponential enhancement of T_K. In the specific context of adatoms on graphene, it was shown[19] that Kondo physics survives the presence of bulk Rashba coupling, with a Kondo temperature that can change faster or slower with tuning of the chemical potential than would be the case in the absence of SO interaction (where the low-energy excitations are massless Dirac fermions).

This paper revisits the Kondo problem in the presence of Rashba SO interaction from a different perspective. We focus on two different scenarios under which the Rashba coupling in a 2DEG might be externally tuned: (1) an open electron system with a Fermi level pinned to that of external reservoirs, and (2) an isolated system with a constant band filling and a Fermi energy that varies with the Rashba coupling. The appropriate model for a magnetic impurity in a Rashba-coupled host is mapped exactly to effective two-channel and one-channel Anderson models without SO interaction but with conduction-band densities of states that

are modified to account for the Rashba coupling. For the specific case of quadratic band dispersion (in the absence of SO interaction) and local impurity-band hybridization, we use the NRG technique to solve the effective one-channel model to calculate thermodynamic properties, from which we extract the Kondo temperature. For fixed Fermi energy, the case considered in previous work, we reproduce the conclusions of Ref. 15 that many-body screening of the impurity is complete, thermodynamic properties have conventional Kondo temperature dependences, and varying the Rashba coupling produces only modest changes in the many-body scale T_K. For fixed band filling, by contrast, increasing the Rashba coupling can drive the system into a helical regime with an increase in the effective density of states at the Fermi level. In the helical regime, thermodynamics retain their conventional nature, but with a characteristic scale T_K that is exponentially enhanced.

We also solve numerically the effective two-channel Anderson model, which retains angular-momentum information that is discarded in the one-channel model. Calculations of static angular-momentum correlations provide explicit confirmation of the expectation from previous works[14–16,18,19] that the SO interaction induces an indirect coupling between the impurity and electrons of nonzero orbital angular momentum.

Entry to the helical regime requires very strong Rashba couplings and/or low carrier densities[3]. There has been considerable recent progress in fabrication of very low-density and clean two-dimensional hole gases[20], but here Coulomb interactions will likely replace disorder as a barrier to reaching the helical regime. However, it has been suggested that this regime may be accessed in a driven system by using circularly polarized light to create an effective Zeeman field that opens a gap between the two Rashba bands[21]. (Similar ideas have been proposed for engineering topological states in insulators[22,23].) Although the breaking of time-reversal symmetry is inimical to the Kondo effect, this proposed experiment offers an opportunity to study Kondo physics in the presence of an effective magnetic field that couples directly only to the bulk electrons.

A real magnetic field would couple both to the spin of the bulk electrons and to the impurity spin, with respective g factors g_b and g_i that need not be equal. There have been numerous studies of Anderson and Kondo models in fields that couple equally to the bulk and impurity spins ($g_b = g_i$) or only to the impurity ($g_b = 0$). Moreover, it is has been shown[24] how to map between Kondo models having different pairs (g_b, g_i) and (g_b', g_i') so long as $g_i \neq 0$ and $g_i' \neq 0$. It is well understood[25] that in such cases, Kondo correlations are destroyed once the conduction-band Zeeman splitting $2\,\epsilon_Z$ becomes comparable[26] to T_K. By contrast, the proposal of Ref. 21 corresponds to a case $g_i = 0$ that has received little attention until now. Under these circumstances, we find (through NRG solution of an effective one-channel Anderson model) that the impurity contribution to the total

angular momentum of the system's ground state is a universal function, not of ϵ_Z/T_K, but rather of $f\,\Gamma\epsilon_Z/T_K D$, where Γ is the hybridization width of the impurity level, D is a measure of the conduction-band width, and the dimensionless quantity f depends on other model parameters: the impurity level energy and on-site Coulomb repulsion, as well as (in this particular realization) the Rashba coupling. A perturbative treatment of field-induced changes in the effective densities of states for electrons with different components of the total angular momentum allows the scaling to be interpreted in terms of an effective spin-splitting of the impurity level by an energy proportional to $\Gamma\epsilon_Z/D$. A similar picture should hold for any realization of the Anderson impurity model with $g_i = 0$, as seems likely to be achievable in lateral quantum dots[27].

The remainder of the paper is organized as follows. Section II describes the Anderson model for a magnetic impurity in a two-dimensional host with bulk Rashba SO interaction, and outlines the mapping of the problem to a one-channel Anderson model with a hybridization function that depends on energy and, in the presence of a bulk Zeeman splitting as proposed in Ref. 21, also on the component of the electron's total angular momentum parallel to the Zeeman field. Explicit expressions for the hybridization function are provided for cases where the band dispersion in the absence of Rashba coupling is purely quadratic. Section III presents numerical results for such cases, focusing on the effect of the Rashba coupling on the Kondo temperature T_K and on static angular-momentum correlations, as well as the variation of the impurity polarization with bulk Zeeman field. We summarize our results in Sec. IV. Appendix A describes a perturbative method used to analyze the effects of Rashba coupling (in Sec. III A 2) and of a bulk Zeeman splitting (in Sec. III B). Details of the calculation of angular-momentum correlations appear in Appendix B.

II. MODEL AND PRELIMINARY ANALYSIS

A. Anderson model with Rashba coupling

We consider an Anderson impurity in a two-dimensional electron gas in the presence of Rashba SO coupling, modeled by the Hamiltonian[15,18]

$$H = H_{\text{bulk}} + H_{\text{imp}} + H_{\text{hyb}}. \tag{1}$$

Here, $H_{\text{bulk}} = H_0 + H_{\text{Rashba}}$, where

$$H_0 = \sum_{\mathbf{k},\sigma} \epsilon(\mathbf{k})\, c_{\mathbf{k},\sigma}^\dagger c_{\mathbf{k},\sigma} \tag{2}$$

describes the conduction band in the absence of SO interaction, with operator $c_{\mathbf{k},\sigma}$ destroying a band electron of two-dimensional wave vector $\mathbf{k} = k_x\hat{\mathbf{x}} + k_y\hat{\mathbf{y}}$, spin z component $\sigma = \pm 1/2$ (or $\uparrow, \downarrow$), and energy $\epsilon(\mathbf{k})$. The second term in H_{bulk} represents the effect of the Rashba

SO interaction $\lambda_R\,\hat{\mathbf{z}}\cdot\boldsymbol{\sigma}\times\mathbf{k}$, where $\boldsymbol{\sigma}/2$ is the electron spin operator:

$$H_{\text{Rashba}} = i\lambda_R \sum_{\mathbf{k}} k\,e^{-i\phi_k} c^{\dagger}_{\mathbf{k},\uparrow} c_{\mathbf{k},\downarrow} + \text{H.c.}, \qquad (3)$$

where $k=|\mathbf{k}|$, $\phi_k=\text{atan}\,(k_y/k_x)$ are the polar components of $\mathbf{k}$, and λ_R is the SO coupling (assumed in our analysis to be non-negative).

In isolation, the nondegenerate impurity level is described by

$$H_{\text{imp}} = (\epsilon_d + \mu)\big(d^{\dagger}_{\uparrow}d_{\uparrow} + d^{\dagger}_{\downarrow}d_{\downarrow}\big) + U d^{\dagger}_{\uparrow}d_{\uparrow}d^{\dagger}_{\downarrow}d_{\downarrow}, \quad (4)$$

where d_σ destroys an electron with spin z component σ and energy ϵ_d relative to the chemical potential μ, and U is the on-site Coulomb repulsion. The impurity state is assumed to exhibit axial symmetry about $\hat{\mathbf{z}}$.

The last term in Eq. (1), representing tunneling of electrons between the impurity and the bulk, is

$$H_{\text{hyb}} = \frac{1}{\sqrt{N_c}} \sum_{\mathbf{k},\sigma} V(\mathbf{k})\big(c^{\dagger}_{\mathbf{k},\sigma}d_\sigma + \text{H.c.}\big), \qquad (5)$$

where N_c is the number of unit cells in the host (and hence the number of distinct $\mathbf{k}$ values in the first Brillouin zone) and the hybridization matrix element $V(\mathbf{k})$ can be taken to be real and non-negative. We note that although the orbital motion of the conduction electrons is constrained to two dimensions, all spin vectors are fully three-dimensional.

For simplicity, we consider a jellium host such that the band dispersion and the hybridization matrix element are isotropic in $\mathbf{k}$ space, i.e., $\epsilon(\mathbf{k})=\epsilon(k)$ and $V(\mathbf{k})=V(k)$.

B. Mapping to a two-channel Anderson model

This section lays out an exact transformation of the Hamiltonian (1) into the form of an effective two-channel Anderson model for a magnetic impurity hybridizing with two bands in which the SO interaction has been subsumed into a modification of the density of states. The mapping generalizes the one presented in Ref. 15 to allow for arbitrary forms of $\epsilon(k)$ and $V(k)$.

We take the thermodynamic limit in the standard manner by letting the unit-cell number $N_c \to \infty$ and the system area $A \to \infty$ in such a way that $A/N_c \to A_c$, a finite unit-cell area. Each summation $\sum_{\mathbf{k}} f(\mathbf{k})$ over a discrete wave vector $\mathbf{k}$ can be replaced by an integral $(A_c/4\pi^2)\int d^2\mathbf{k}\,f(\mathbf{k})$.

In the absence of SO coupling, it is natural to adopt a basis of states having a definite z component of the orbital angular momentum about the impurity site. The transformation[14,28]

$$c_{\mathbf{k},\sigma} \to \sum_{m=-\infty}^{\infty} \sqrt{\frac{2\pi}{A_c k}}\, e^{im(\phi_k-\pi/2)}\, c_{k,m,\sigma}, \qquad (6)$$

where $\{c_{k,m,\sigma}, c^{\dagger}_{k',m',\sigma'}\}=\delta(k-k')\,\delta_{m,m'}\delta_{\sigma,\sigma'}$, allows one to rewrite Eq. (2) in the diagonal form

$$H_0 = \sum_{m,\sigma} \int dk\,\epsilon(k)\,c^{\dagger}_{k,m,\sigma}\,c_{k,m,\sigma}, \qquad (7)$$

while the hybridization term becomes

$$H_{\text{hyb}} = \sqrt{\frac{A_c}{2\pi}} \int dk\,\sqrt{k}\,V(k)\big(c^{\dagger}_{k,0,\sigma}d_\sigma + \text{H.c.}\big), \qquad (8)$$

in which the impurity couples only to the $m=0$ mode.

The Rashba Hamiltonian term, which becomes

$$H_{\text{Rashba}} = \lambda_R \int dk\,k \sum_m c^{\dagger}_{k,m,\uparrow} c_{k,m+1,\downarrow} + \text{H.c.}, \quad (9)$$

is not diagonal in the (k,m,σ) basis because Rashba SO interaction couples spin and orbital degrees of freedom. However, since H_{Rashba} mixes only pairs of states $(k,m,\uparrow)$ and $(k,m+1,\downarrow)$, H_{bulk} conserves $\tau=m+\sigma$, the z component of total (orbital plus spin) angular momentum. The bulk Hamiltonian also commutes with the helicity operator

$$\hat{h} = \hat{\mathbf{z}}\cdot\boldsymbol{\sigma}\times\hat{\mathbf{k}} = \int dk\,\sum_m c^{\dagger}_{k,m,\uparrow}\,c_{k,m+1,\downarrow} + \text{H.c.} \quad (10)$$

It is therefore convenient to perform a canonical transformation to a new complete basis of fermionic operators

$$\tilde{c}_{k,h,\tau} = \frac{1}{\sqrt{2}}\big(h^{\tau-1/2}\,c_{k,\tau-1/2,\uparrow} + h^{\tau+1/2}\,c_{k,\tau+1/2,\downarrow}\big), \quad (11)$$

each of which annihilates an electron in a state of well-defined $\tau=\pm1/2,\,\pm3/2,\dots$ and definite helicity $h=\pm1$ (abbreviated $h=\pm$ at certain points below).

This transformation diagonalizes the bulk Hamiltonian, yielding

$$H_{\text{bulk}} = \sum_{h,\tau} \int dk\,\epsilon_h(k)\,\tilde{c}^{\dagger}_{k,h,\tau}\,\tilde{c}_{k,h,\tau} \qquad (12)$$

with a helicity-dependent (but total-angular-momentum-independent) dispersion

$$\epsilon_h(k) = \epsilon(k) + h\lambda_R k. \qquad (13)$$

The two operators $c_{k0\sigma}$ to which the impurity couples in Eq. (8) can be represented in terms of four operators $\tilde{c}_{k,h,\tau}$, namely those with $h=\pm$ and $\tau=\pm1/2$. Since these four operators also involve $c_{k,-1,\uparrow}$ and $c_{k,1,\downarrow}$, one sees that the Rashba SO interaction creates an indirect coupling of the impurity to conduction electrons with nonzero orbital angular momentum[14,18].

One can drop the uninteresting contribution to H_{bulk} from electrons having total angular momentum z component $|\tau|>1/2$, thereby reducing Eq. (1) to a two-channel Anderson Hamiltonian with the helicity h acting

as a channel index:

$$H = \sum_{h,\tau} \int dk\, \epsilon_h(k)\, \tilde{c}^\dagger_{k,h,\tau} \tilde{c}_{k,h,\tau} + H_{\text{imp}}$$

$$+ \sqrt{\frac{A_c}{4\pi}} \sum_{h,\tau} \int dk\, \sqrt{k}\, V(k)\, (\tilde{c}^\dagger_{k,h,\tau} d_\tau + \text{H.c.}). \quad (14)$$

Due to the difference $\epsilon_+(k) - \epsilon_-(k) = 2\lambda_R k$, the two helicities enter Eq. (14) in an inequivalent manner; in particular, they have different Fermi wave vectors. It is also important to bear in mind that the index $\tau = \pm 1/2$ (or $\uparrow$, $\downarrow$) labels the z component of the total angular momentum, although this reduces to the z component of spin for the impurity operators d_τ.

Equation (14) can be transformed to an energy representation by defining

$$\tilde{c}_{\epsilon,h,j,\tau} = |\epsilon'_h(k_j)|^{-1/2}\, \tilde{c}_{k_j,h,\tau}, \quad (15)$$

where $\epsilon'_h = d\epsilon_h/dk$ and $k_j(\epsilon,h)$, $j = 1, \ldots, n_h(\epsilon)$ are the numerically distinct roots of the equation $\epsilon_h(k_j) = \epsilon$. If $\epsilon_h(k)$ is a monotonically increasing function of k, as would be the case for free fermions in the absence of SO interaction, then $n_h(\epsilon) = 0$ for $\epsilon < \epsilon_h(0)$ and $n_h(\epsilon) = 1$ for $\epsilon \geq \epsilon_h(0)$. However, as discussed in greater detail in Sec. II E, the presence of Rashba SO interaction creates an energy range within which $n_-(\epsilon) = 2$.

The operators defined in Eq. (15) obey the canonical anticommutation relations

$$\{\tilde{c}_{\epsilon,h,j,\tau}, \tilde{c}^\dagger_{\epsilon',h',j',\tau'}\} = \delta(\epsilon - \epsilon')\, \delta_{h,h'}\, \delta_{j,j'}\, \delta_{\tau,\tau'} \quad (16)$$

and allow Eq. (14) to be rewritten

$$H = \sum_{h,\tau} \int d\epsilon\, \epsilon \sum_{j=1}^{n_h(\epsilon)} \tilde{c}^\dagger_{\epsilon,h,j,\tau} \tilde{c}_{\epsilon,h,j,\tau} + H_{\text{imp}}$$

$$+ \sum_{h,\tau} \int d\epsilon \sum_{j=1}^{n_h(\epsilon)} \sqrt{\Gamma_{h,j}(\epsilon)/\pi}\, (\tilde{c}^\dagger_{\epsilon,h,j,\tau} d_\tau + \text{H.c.}), \quad (17)$$

where

$$\Gamma_{h,j}(\epsilon) = \frac{A_c\, k_j}{4|\epsilon'_h(k_j)|}\, V(k_j)^2 \quad (18)$$

is the contribution to the helicity-h hybridization function at energy ϵ that arises from wave vector $k = k_j(\epsilon, h)$.

Equation (17) is an exact restatement of Eq. (14), and allows full recovery of dependences on the radial coordinate measured from the impurity site, as obtained via Fourier transformation with respect to k. Further transformations of the Hamiltonian described in Sec. II C below serve to simplify the calculation of certain thermodynamic properties, but necessarily entail loss of information about radial or angular momentum degrees of freedom that could be inferred from a complete solution of Eq. (17).

C. Further reduction of the model

One simplification of Eq. (17) arises from noting that for energies ϵ where $n_h(\epsilon) > 1$, the impurity couples to a single linear combination of the operators $\tilde{c}_{\epsilon h j \tau}$, $j = 1, 2, \ldots, n_h(\epsilon)$. Defining

$$\sqrt{\Gamma_h(\epsilon)}\, \tilde{c}_{\epsilon,h,\tau} = \sum_{j=1}^{n_h(\epsilon)} \sqrt{\Gamma_{h,j}(\epsilon)}\, \tilde{c}_{\epsilon,h,j,\tau} \quad (19)$$

with a helicity-h hybridization function

$$\Gamma_h(\epsilon) = \sum_{j=1}^{n_h(\epsilon)} \Gamma_{h,j}(\epsilon) \quad (20)$$

allows one to write

$$H = \sum_{h,\tau} \int d\epsilon\, \epsilon\, \tilde{c}^\dagger_{\epsilon,h,\tau} \tilde{c}_{\epsilon,h,\tau} + H_{\text{imp}}$$

$$+ \sum_{h,\tau} \int d\epsilon\, \sqrt{\Gamma_h(\epsilon)/\pi}\, (\tilde{c}^\dagger_{\epsilon,h,\tau} d_\tau + \text{H.c.}), \quad (21)$$

from which have been dropped diagonal terms involving $n_h(\epsilon) - 1$ linear combinations of the operators $\tilde{c}_{\epsilon,h,j,\tau}$ that are orthogonal to $\tilde{c}_{\epsilon,h,\tau}$. The mapping from $n_h(\epsilon) > 1$ operators $\tilde{c}_{\epsilon,h,j,\tau}$ to a single $\tilde{c}_{\epsilon,h,\tau}$ involves loss of radial information since the latter operator cannot be associated with any single wave vector k.

Another simplification can be made by combining the $h = +$ and $h = -$ states of the same energy that couple to the impurity. Defining

$$\sqrt{\Gamma(\epsilon)}\, \tilde{c}_{\epsilon,\tau} = \sqrt{\Gamma_+(\epsilon)}\, \tilde{c}_{\epsilon,+,\tau} + \sqrt{\Gamma_-(\epsilon)}\, \tilde{c}_{\epsilon,-,\tau} \quad (22)$$

with a total hybridization function

$$\Gamma(\epsilon) = \Gamma_+(\epsilon) + \Gamma_-(\epsilon), \quad (23)$$

one can again discard decoupled degrees of freedom [here, associated with $\sqrt{\Gamma_-(\epsilon)}\, \tilde{c}_{\epsilon,+,\tau} - \sqrt{\Gamma_+(\epsilon)}\, \tilde{c}_{\epsilon,-,\tau}$] to arrive at an effective one-impurity Anderson model

$$H = \sum_\tau \int d\epsilon\, \epsilon\, \tilde{c}^\dagger_{\epsilon,\tau} \tilde{c}_{\epsilon,\tau} + H_{\text{imp}}$$

$$+ \sum_\tau \int d\epsilon\, \sqrt{\Gamma(\epsilon)/\pi}\, (\tilde{c}^\dagger_{\epsilon,\tau} d_\tau + \text{H.c.}). \quad (24)$$

That the original model in Eq. (1) can be reduced to a one-channel Anderson impurity model was shown previously in Ref. 15 for the specific case of a quadratic $\epsilon(k)$ and a local (k-independent) $V(k)$. However, the derivation above makes clear that the price paid for going from Eq. (21) to Eq. (24) is the loss of the ability to distinguish between the spin and orbital angular momenta within a bulk state of given z component of the total angular momentum. For this reason, Sec. III presents not only

impurity properties calculated from Eq. (24), but also impurity-bulk angular-momentum correlations obtained via numerical solution of Eq. (21).

In the absence of the impurity, the bands entering Eqs. (21) and (24) would be filled at temperature $T = 0$ up to a chemical potential $\mu = \epsilon_F$. (As will be emphasized in Secs. II E and III, the Fermi energy ϵ_F may or may not take the same value as for $\alpha = 0$, depending on the experimental setup being described.) In cases where $\Gamma(-\epsilon_d) \ll -\epsilon_d$ and $\Gamma(U + \epsilon_d) \ll U + \epsilon_d$, it is appropriate to apply a generalized Schrieffer-Wolff transformation[17] to map the two- and one-channel Anderson models to two- and one-channel Kondo models, respectively. In general, the resulting Kondo models[18] will not be the same as those obtained by starting with a Kondo Hamiltonian for a magnetic impurity in a 2DEG and then incorporating a bulk Rashba SO interaction.

D. Model with bulk Zeeman field

In a recent paper, Ojanen and Kitagawa[21] proposed to realize a helical system through irradiation of a two-dimensional electron gas containing Rashba SO interaction by light in the THz frequency range. After time-averaging over a period of the electromagnetic radiation, the bulk electrons experience an effective Zeeman coupling of tunable strength $\epsilon_Z = (\lambda_R e E_0)^2/\Omega^3$, where E_0 and $\Omega/2\pi$ are the magnitude and frequency of the applied electric field. Provided that the characteristic rate $k_B T_K/2\pi$[26] of spin flips involved in Kondo screening is much slower than $\Omega/2\pi$, the impurity will effectively interact with the time-averaged band structure. This regime spans $T_K \ll 50\,\mathrm{K}$ for $\Omega/2\pi = 1\,\mathrm{THz}$ and $T_K \ll 500\,\mathrm{K}$ for $\Omega/2\pi = 10\,\mathrm{THz}$, conditions that will be readily satisfied in most experiments. We also note that for the values of E_0 envisioned in Ref. 21, the magnetic component of the circularly polarized light is so small as to have negligible effect.

With this motivation, we consider the Hamiltonian (1) augmented by a term

$$H_{\mathrm{Zeeman}} = 2\epsilon_Z \sum_{\mathbf{k},\sigma} \sigma \, c_{\mathbf{k},\sigma}^\dagger c_{\mathbf{k},\sigma}, \qquad (25)$$

where $\sigma = \pm 1/2$ or $\uparrow, \downarrow$, depending on the context, and we assume below that $\epsilon_Z \geq 0$. The model can again be mapped to effective two-channel and one-channel Anderson models via a sequence of steps along the lines laid out in Secs. II B and II C.

In order to diagonalize $H_{\mathrm{bulk}} = H_0 + H_{\mathrm{Rashba}} + H_{\mathrm{Zeeman}}$, the operator transformation in Eq. (11) must be generalized to

$$\tilde{c}_{k,h,\tau} = \frac{1}{\sqrt{2}} \big[h^{\tau-1/2} \beta_h(k) \, c_{k,\tau-1/2,\uparrow} \qquad (26)$$
$$+ h^{\tau+1/2} \beta_{-h}(k) \, c_{k,\tau+1/2,\downarrow} \big],$$

where

$$\beta_{\pm 1}(k) = \sqrt{1 \pm \frac{\epsilon_Z}{(\lambda_R^2 k^2 + \epsilon_Z^2)^{1/2}}} \,. \qquad (27)$$

This yields Eq. (12) with a helicity-dependent dispersion

$$\epsilon_h(k) = \epsilon(k) + h\sqrt{\lambda_R^2 k^2 + \epsilon_Z^2} \qquad (28)$$

that features a gap $2\,\epsilon_Z$ at $k = 0$, while the impurity-bulk hybridization becomes

$$H_{\mathrm{hyb}} = \sqrt{\frac{A_c}{4\pi}} \sum_{h,\tau} \int dk \, \sqrt{k} \, V(k) \, \beta_{2\tau h}(k) \left(\tilde{c}_{k,h,\tau}^\dagger \, d_\tau + \mathrm{H.c.} \right), \qquad (29)$$

where the value of the product $2\tau h = \pm 1$ selects between the two functions $\beta_{\pm 1}(k)$ defined in Eq. (27). After further transformation to an energy representation, the problem maps to a generalized two-channel Anderson model

$$H = \sum_{h,\tau} \int d\epsilon \, \epsilon \, \tilde{c}_{\epsilon,h,\tau}^\dagger \, \tilde{c}_{\epsilon,h,\tau} + H_{\mathrm{imp}}$$
$$+ \sum_{h,\tau} \int d\epsilon \, \sqrt{\Gamma_{h,\tau}(\epsilon)/\pi} \left(\tilde{c}_{\epsilon,h,\tau}^\dagger \, d_\tau + \mathrm{H.c.} \right), \qquad (30)$$

containing a helicity- and angular-momentum-dependent hybridization function

$$\Gamma_{h,\tau}(\epsilon) = \sum_{j=1}^{n_h(\epsilon)} \frac{A_c \, k_j}{4|\epsilon_h'(k_j)|} \left[\beta_{2\tau h}(k_j) \, V(k_j) \right]^2. \qquad (31)$$

Here, $k_j(\epsilon, h)$, $j = 1, \ldots, n_h(\epsilon)$ are the distinct roots of the equation $\epsilon_h(k_j) = \epsilon$ for the gapped dispersion in Eq. (28).

As before, the two-channel Anderson model can be mapped into an effective one-channel model. It is straightforward to show that the impurity couples only to the linear combination of operators defined via

$$\sqrt{\Gamma_\tau(\epsilon)} \, \tilde{c}_{\epsilon,\tau} = \sqrt{\Gamma_{+,\tau}(\epsilon)} \, \tilde{c}_{\epsilon,+,\tau} + \sqrt{\Gamma_{-,\tau}(\epsilon)} \, \tilde{c}_{\epsilon,-,\tau} \qquad (32)$$

with

$$\Gamma_\tau(\epsilon) = \Gamma_{+,\tau}(\epsilon) + \Gamma_{-,\tau}(\epsilon), \qquad (33)$$

leading to a Hamiltonian

$$H = \sum_\tau \int d\epsilon \, \epsilon \, \tilde{c}_{\epsilon,\tau}^\dagger \, \tilde{c}_{\epsilon,\tau} + H_{\mathrm{imp}}$$
$$+ \sum_\tau \int d\epsilon \, \sqrt{\Gamma_\tau(\epsilon)/\pi} \left(\tilde{c}_{\epsilon,\tau}^\dagger \, d_\tau + \mathrm{H.c.} \right). \qquad (34)$$

Comparison with Eq. (24) shows that the effect the Zeeman field is subsumed into an angular-momentum dependence of the hybridization function.
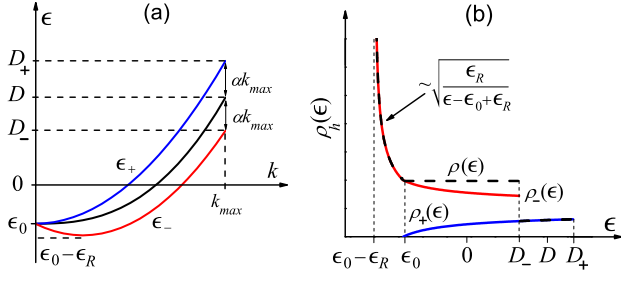
FIG. 1. (Color online) Schematic plots of (a) the dispersion relations $\epsilon_h(k)$ and (b) the densities of states per helicity channel $\rho_h(\epsilon)$, in the presence of Rashba SO interaction. The middle curve in (a) represents the dispersion $\epsilon(k)$ in the absence of Rashba interaction. In (b), the combined density of states $\rho(\epsilon)$ (dashed line) is constant and equal to its no-Rashba value $\rho_0(\epsilon)$ throughout the energy range $\epsilon_0 < \epsilon < D_-$.

E. Local hybridization and quadratic band dispersion

The band dispersion $\epsilon(k)$, the hybridization matrix element $V(k)$, and the Zeeman energy ϵ_Z enter Eqs. (30) and (34) only in combination through the hybridization functions $\Gamma_{h,\tau}(\epsilon)$, which reduce to $\Gamma_h(\epsilon)$ for $\epsilon_Z = 0$. Henceforth, we will assume that the hybridization is local, i.e., $V(k) = V$, in which case each hybridization function can be written as an energy-independent prefactor πV^2 times an appropriately resolved density of states per unit cell. For example,

$$\Gamma_{h,\tau}(\epsilon) = \pi \rho_{h,\tau}(\epsilon) V^2 \qquad (35)$$

where $\rho_{h,\tau}(\epsilon)$ is the density of states per unit cell for helicity-h and total angular momentum z component τ.

We also specialize to cases in which the band dispersion in the absence of SO interaction takes the purely parabolic form[15,26] $\epsilon(k) = \epsilon_0 + k^2/2m^*$, where m^* is the effective mass and $\epsilon_0 \leq 0$ is the position of the bottom of the band relative to the Fermi energy $\epsilon_F = 0$. This dispersion yields the density of states (per unit cell, per spin orientation)

$$\rho_0(\epsilon) = \frac{A_c k}{2\pi |d\epsilon/dk|} = \varrho_0\, \Theta(\epsilon - \epsilon_0)\, \Theta(D - \epsilon) \qquad (36)$$

where $\varrho_0 = A_c m^*/(2\pi)$ and $D \equiv \epsilon(k_{\max}) = \epsilon_0 + \varrho_0^{-1}$ is an upper cutoff introduced to enforce $\int_{-\infty}^{\infty} \rho(\epsilon)\, d\epsilon = 1$. We consider situations where the band is less than half-filled (i.e., $|\epsilon_0| < D$) and take D to be the fundamental energy scale in the problem.

When Rashba SO interaction is taken into account, the helicity-h dispersion defined in Eq. (13) can be expressed as

$$\epsilon_h(k) = \tilde{\epsilon}_0 + \frac{(k + h k_R)^2}{2m^*}, \qquad (37)$$

where it is convenient to define a Rashba wave vector $k_R = m^* \lambda_R$ and a Rashba energy $\epsilon_R = k_R^2/2m^* =$
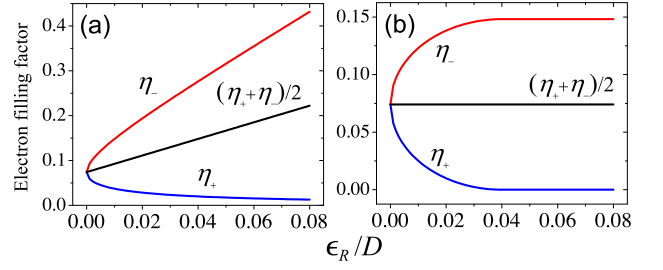

FIG. 2. (Color online) Helicity-resolved conduction-band filling fractions $\eta_\pm$ and overall filling fraction $\eta = (\eta_+ + \eta_-)/2$, plotted as functions of Rashba energy ϵ_R for $\epsilon_0 = -0.08D$ and (a) fixed Fermi energy $\epsilon_F = 0$, (b) constant filling fraction $\eta = -\epsilon_0/(D - \epsilon_0) \approx 0.074$.

$m^* \lambda_R^2/2 = \lambda_R k_R/2$, such that $\tilde{\epsilon}_0 = \epsilon_0 - \epsilon_R$ is the energy at a parabolic minimum in $\epsilon_-(k)$ located at $k = k_R$. These dispersions, plotted schematically in Fig. 1(a), yield helicity-resolved densities of states (per unit cell, per total angular momentum z component)

$$\rho_h(\epsilon) = \begin{cases} \varrho_0\, \dfrac{\epsilon_R}{\sqrt{\epsilon_R(\epsilon - \tilde{\epsilon}_0)}}\, \delta_{h,-} & \text{for } \tilde{\epsilon}_0 < \epsilon < \epsilon_0, \\[2mm] \dfrac{\varrho_0}{2}\left[1 - h\, \dfrac{\epsilon_R}{\sqrt{\epsilon_R(\epsilon - \tilde{\epsilon}_0)}}\right] & \text{for } \epsilon_0 < \epsilon < D_h, \\[2mm] 0 & \text{otherwise.} \end{cases} \qquad (38)$$

The upper cutoff of the helicity-h band has shifted from D to $D_h = \epsilon_h(k_{\max}) = D + 2h\sqrt{\epsilon_R(D - \epsilon_0)}$ such that $\int_{-\infty}^{\infty} \rho_h(\epsilon)\, d\epsilon = \frac{1}{2}$. The densities of states $\rho_h(\epsilon)$ are plotted schematically in Fig. 1(b). When compared with $\frac{1}{2}\rho_0(\epsilon)$ [to which $\rho_+(\epsilon)$ and $\rho_-(\epsilon)$ reduce for $\epsilon_R = 0$], the most striking features are (i) the shift of $h = +$ states to higher energies $D < \epsilon < D_+$, resulting in a monotonic depression of $\rho_+(\epsilon)$ to zero as $\epsilon \to 0^+$, and (ii) the shift of $h = -$ states from $D_- < \epsilon < D$ to lower energies, and particularly the $1/\sqrt{\epsilon - \tilde{\epsilon}_0}$ variation of $\rho_-(\epsilon)$ over the range $\tilde{\epsilon}_0 < \epsilon < \epsilon_0$. The van Hove singularity in $\rho_-(\epsilon)$ at $\epsilon = \tilde{\epsilon}_0$ arises from the parabolic minimum in $\epsilon_-(k)$ at $k = k_R$.

Figure 1(b) also shows (dashed line) the density of states $\rho(\epsilon) = \rho_+(\epsilon) + \rho_-(\epsilon)$ for the effective one-channel Anderson problem defined in Eq. (24). This function is identical to its counterpart in the absence of Rashba interaction over a wide energy window $0 \leq \epsilon \leq D_-$, with $\rho(\epsilon)$ differing from ρ_0 only in the redistribution of weight around the upper band edge ($\epsilon > D_-$), with part of that weight being transferred into the low-energy upturn spanning $\tilde{\epsilon}_0 < \epsilon < \epsilon_0$.

In Sec. III, we examine the effect of increasing the Rashba energy ϵ_R, as might be achieved experimentally by increasing the strength of an electric field applied perpendicularly to the two-dimensional electron gas. We consider two scenarios:

(1) The Fermi energy is fixed at $\epsilon_F = 0$, as would be the

case if the system were maintained in equilibrium with a reservoir of electrons at fixed chemical potential. As illustrated in Fig. 2(a), the filling fraction of each helicity band, $\eta_h = 2 \int_{-\infty}^{\epsilon_F} \rho_h(\epsilon)\, d\epsilon$, changes with the Rashba energy in such a way that the overall filling fraction increases linearly with ϵ_R:

$$\eta = \tfrac{1}{2}(\eta_+ + \eta_-) = \frac{2\,\epsilon_R - \epsilon_0}{D - \epsilon_0}. \qquad (39)$$

(2) The overall band filling is held constant, as would occur if the system were isolated from any external source of electrons. In this case, as illustrated in Fig. 2(b), varying the Rashba coupling still leads to changes in η_+ and η_-, but it does not alter their mean $\eta = -\epsilon_0/(D - \epsilon_0)$. This comes about because with increasing ϵ_R, the Fermi energy decreases according to

$$\epsilon_F(\epsilon_R) = \begin{cases} -2\,\epsilon_R & \epsilon_R < |\epsilon_0|/2, \\ \epsilon_0 - \epsilon_R + \epsilon_0^2/4\epsilon_R & \epsilon_R \geq |\epsilon_0|/2. \end{cases} \qquad (40)$$

For $\epsilon_R > |\epsilon_0|/2$, the Fermi energy lies below ϵ_0, with two important consequences. First, the occupied bulk states all have $h = -$, resulting in the formation of an unconventional, helical metal. Second, the total density of states at the Fermi level is $\rho(\epsilon_F) = 2\varrho_0\epsilon_R/|\epsilon_0|$, which is enhanced over its value ϱ_0 for $\epsilon_R = 0$. This situation is unlikely to be realized in standard III-V semiconductor heterostructures[3], since it would require very high Rashba couplings or very low carrier densities that will be affected by disorder or Coulomb interactions. However, driven systems may allow investigation of this interesting regime provided that one takes into account the effective Zeeman splitting of the helicity-resolved bands[21].

In the presence of a bulk Zeeman field as well as Rashba interaction, the helicity-h dispersion in Eq. (28) can be expressed as

$$\epsilon_h(k) = \tilde{\epsilon}_0 + \frac{(\sqrt{k^2 + k_Z^2} + hk_R)^2}{2m^*}, \qquad (41)$$

where $k_Z = \epsilon_Z/\lambda_R$ and we have redefined

$$\tilde{\epsilon}_0 = \epsilon_0 - \epsilon_R - \frac{\epsilon_Z^2}{4\epsilon_R} = \epsilon_0 - \epsilon_Z - \frac{(2\epsilon_R - \epsilon_Z)^2}{4\epsilon_R}. \qquad (42)$$

Equation (41) implies that $\epsilon_+(k)$ rises monotonically with increasing k from $\epsilon_+(0) = \epsilon_0 + \epsilon_Z$. If $k_Z < k_R$, which is equivalent to the condition $\epsilon_Z < 2\epsilon_R$, the $h = -$ dispersion has a parabolic minimum at a nonzero wave vector $k = \sqrt{k_R^2 - k_Z^2}$, as shown schematically in Fig. 3(a); otherwise, $\epsilon_-(k)$ rises monotonically from $\epsilon_-(0) = \epsilon_0 - \epsilon_Z$, with a small-$k$ behavior that is quartic in k for $\epsilon_Z = 2\epsilon_R$ but quadratic for any $\epsilon_Z > 2\epsilon_R$ [see Fig. 3(b)].

The helicity- and angular-momentum-resolved densities of states entering Eq. (35) become

$$\rho_{h,\tau}(\epsilon) = \begin{cases} \varrho_0 \dfrac{\epsilon_R - \tau\epsilon_Z}{\sqrt{\epsilon_R(\epsilon - \tilde{\epsilon}_0)}}\, \Theta(2\,\epsilon_R - \epsilon_Z)\, \delta_{h,-} & \text{for } \tilde{\epsilon}_0 < \epsilon < \epsilon_0 - \epsilon_Z, \\[2ex] \dfrac{\varrho_0}{2}\left[1 - h\,\dfrac{\epsilon_R - \tau\epsilon_Z}{\sqrt{\epsilon_R(\epsilon - \tilde{\epsilon}_0)}}\right] & \text{for } \epsilon_0 + h\epsilon_Z < \epsilon < D_h. \\[2ex] 0 & \text{otherwise,} \end{cases} \qquad (43)$$

where $D_h = D + 2h\sqrt{\epsilon_R(D - \epsilon_R - \tilde{\epsilon}_0)}$. For weak Zeeman splittings $\epsilon_Z \leq 2\,\epsilon_R$, $\rho_{-,\tau}(\epsilon)$ features a van Hove singularity at $\epsilon = \tilde{\epsilon}_0$, associated with the minimum in $\epsilon_-(k)$. By contrast, for strong Zeeman splittings $\epsilon_Z > 2\epsilon_R$, there is no divergence of any $\rho_{h,\tau}(\epsilon)$.

Figures 3 also shows schematic plots of the angular-momentum-resolved densities of states $\rho_\tau(\epsilon) = \sum_h \rho_{h,\tau}(\epsilon)$, which determine $\Gamma_\tau(\epsilon)$ entering Eq. (34). These densities of states coincide with $\rho_0(\epsilon)$ over the energy range $\epsilon_0 + \epsilon_Z < \epsilon < D_-$. For $\epsilon_Z \leq 2\epsilon_R$, each density of states, plotted schematically in Fig. 3(c), inherits a van Hove singularity at $\epsilon = \tilde{\epsilon}_0$ from the divergence of $\rho_{-,\tau}(\epsilon)$. In addition, $\rho_{-1/2}(\epsilon)$ exhibits a jump as the energy drops below $\epsilon = \epsilon_0 - \epsilon_Z$ due to the onset of contributions from $h = -$ states close to $k = 0$. [There is no corresponding jump in $\rho_{1/2}(\epsilon)$ because $\beta_{-1}(k)$ vanishes at $k = 0$.] For $\epsilon_Z > 2\epsilon_R$, by contrast, $\rho_{1/2}(\epsilon)$ approaches zero and $\rho_{-1/2}(\epsilon)$ rises smoothly to a constant limiting value as ϵ approaches $\epsilon_0 - \epsilon_Z$ from above, and both densities of states vanish for $\epsilon < \epsilon_0 - \epsilon_Z$, as sketched in Fig. 3(d).

III. NUMERICAL RESULTS

In order to study Hamiltonians (21), (24), and (34) with the densities of states defined in Eqs. (38) and (43), we have applied the numerical renormalization-group (NRG) method for the solution of the Anderson model[29], as adapted to treat arbitrary densities of states[30,31]. We set the Wilson discretization parameter to $\Lambda = 2.5$, retaining at least $2\,000$ many-body states after each iteration. Results are shown for $\epsilon_0 = -0.08D$ and various combinations of U, ϵ_d, and the hybridization width $\Gamma \equiv \pi\varrho_0 V^2$. Any value of Γ employed in
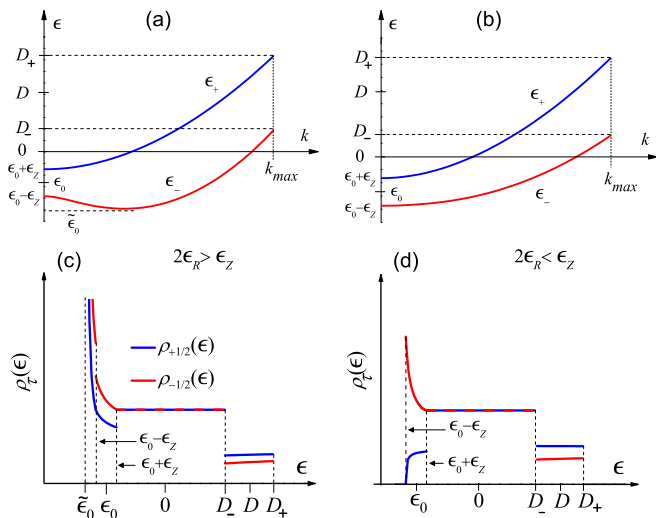
FIG. 3. (Color online) Schematic plots of the effective angular-momentum-resolved densities of states $\rho_\tau(\epsilon)$ obtained from Eq. (43) for (a) weak Zeeman splitting $\epsilon_Z < 2\,\epsilon_R$, (b) strong Zeeman splitting $\epsilon_Z > 2\,\epsilon_R$. In both panels, $\rho_\tau(\epsilon)$ is constant and equal to its no-Rashba value $\rho_0(\epsilon)$ throughout the energy range $\epsilon_0 + \epsilon_Z < \epsilon < D_-$.

an NRG calculation should be equivalent in the continuum limit to a hybridization width $\Gamma_{\mathrm{eff}} = \Gamma/A_\Lambda$, where $A_\Lambda = \frac{1}{2}(\ln \Lambda)(\Lambda + 1)/(\Lambda - 1) \simeq 1.069$ accounts for a reduction in the density of states that arises from the NRG discretization[29].

The results shown in Sec. III A 3 were obtained by solving the two-channel Anderson model [Eq. (21)]. All other data presented in this section come from calculations performed on a one-channel model [either Eq. (24) or Eq. (34)].

A. Results without a Zeeman field

1. Thermodynamic properties

We begin by showing the temperature variation of the impurity contribution to two thermodynamic quantities calculated using the effective one-channel Anderson model [Eq. (24)]: the magnetic susceptibility χ_{imp} (calculated for equal impurity and band g factors, $g_i = g_b$) and the entropy S_{imp}. To reduce NRG discretization errors, we employed interleaved averaging[32] over three different band discretizations.

In order to investigate the universality of the low-temperature physics, Fig. 4 shows $T\chi_{\mathrm{imp}}$ and S_{imp} for a symmetric impurity ($U = -2\epsilon_d = 0.1D$, $\Gamma = 0.005D$) as functions of T/T_K. Note that we have defined χ_{imp} to be the impurity contribution to the static part of the correlation function for the z component of the total angular momentum, which reduces to the customary static spin susceptibility in the case $\epsilon_R = 0$. The Kondo temperature
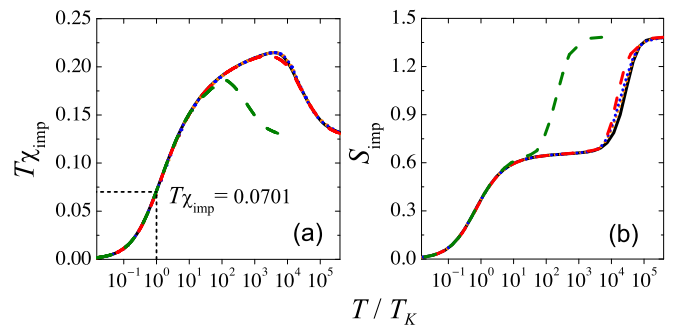

FIG. 4. (Color online) Impurity contribution to (a) temperature times magnetic susceptibility $T\chi_{\mathrm{imp}}$, and (b) entropy S_{imp}, both plotted vs scaled temperature T/T_K for five different cases: a no-Rashba reference (black solid line), and Rashba energies $\epsilon_R/D = 0.04$ (red and orange curves) and 0.08 (green and blue curves) under the scenarios of fixed Fermi energy (dotted lines) and constant band filling (dashed lines). The two dotted lines lie directly on top of one another on the scale of this plot. The Kondo temperature T_K is as defined in Eq. (44). Data are for $\epsilon_0 = -0.08D$, $U = -2\epsilon_d = 0.1D$, and $\Gamma = 0.005D$.

T_K was determined via the conventional criterion[26,29]

$$T_K \chi_{\mathrm{imp}}(T_K) = 0.0701, \qquad (44)$$

or equivalently, via the condition $S_{\mathrm{imp}}(T_K) = 0.383$. The fact that for $T \lesssim T_K$ the curves for $\epsilon_R/D = 0.04$ and 0.08, calculated both for fixed Fermi energy (dotted lines) and for constant band-filling (dashed lines), lie on top of the curve for $\epsilon_R = 0$ (solid line) provides evidence that the low-temperature thermodynamic properties are those of a conventional Kondo effect, with $\lim_{T\to 0} T\chi_{\mathrm{imp}} = 0$ and $\lim_{T\to 0} S_{\mathrm{imp}} = 0$ indicating complete ground-state screening of the impurity degree of freedom.

Even well above the Kondo temperature, four of the five curves in each panel of Fig. 4 are virtually indistinguishable, exhibiting both a high-temperature free-impurity regime (in which $T\chi_{\mathrm{imp}} \simeq 1/8$, $S_{\mathrm{imp}} \simeq \ln 4$) and an intermediate-temperature local-moment regime (where $T\chi_{\mathrm{imp}} \simeq 1/4$, $S_{\mathrm{imp}} \simeq \ln 2$). The only exception is the curve for $\epsilon_R = 0.08D$ at constant band filling. Here, the Fermi energy is pushed down into the van Hove singularity in the effective one-channel density of states. The enhanced hybridization width drives the system from its local-moment regime into mixed valence, where $T\chi_{\mathrm{imp}}$ never rises close to $1/4$ and with decreasing temperature S_{imp} drops from $\ln 4$ to 0 with at most a weak shoulder around $\ln 2$.

2. Kondo temperature

Given that the low-temperature physics is characterized by a single scale T_K, we now examine more closely the effect of Rashba coupling on the Kondo temperature. Figures 5(a) and 6(a) plot the ratio of the Kondo tem-
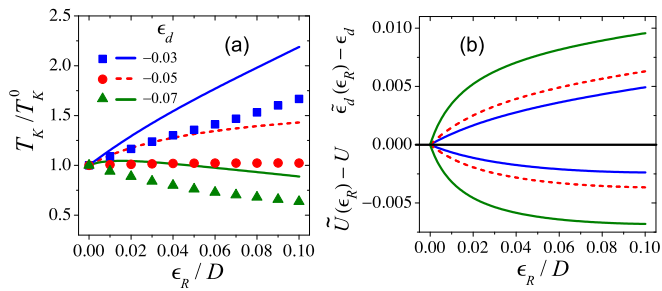
FIG. 5. (Color online) (a) Scaled Kondo temperature T_K/T_K^0 vs Rashba energy ϵ_R for fixed Fermi energy $\epsilon_F = 0$ and for different values of ϵ_d expressed in the legend in units of D. Symbols represent NRG data and lines are the result of the perturbative treatment described in the text. (b) Perturbative shifts $\tilde{\epsilon}_d - \epsilon_d$ and $\tilde{U} - U$ in the effective impurity parameters vs ϵ_R for the same cases shown in (a). Data are for $\epsilon_0 = -0.08D$, $U = 0.1D$, and $\Gamma = 0.005D$.

perature T_K at Rashba energy ϵ_R to its value T_K^0 in the absence of SO interaction.

Figure 5 treats the scenario of fixed Fermi energy $\epsilon_F = 0$ for $\epsilon_0 = -0.08D$, $U = 0.1D$, and $\Gamma = 0.005D$. The Kondo temperature in the absence of SO interaction varies with ϵ_d, taking its smallest value around $\epsilon_d = -U/2 = -0.05D$, for which case $T_K^0 \simeq 1.7 \times 10^{-6}D$. This is very close to the value $1.4 \times 10^{-6}D$ given by substituting $\Gamma(\epsilon_F) = \Gamma_{\text{eff}}$ into Haldane's estimate[26,33]

$$T_K \simeq 0.29 \sqrt{U\,\Gamma(\epsilon_F)} \exp\left[\frac{\pi\epsilon_d(U + \epsilon_d)}{2U\,\Gamma(\epsilon_F)} \right]. \qquad (45)$$

for the Kondo temperature of an Anderson impurity in the limit that $0 < \Gamma(\epsilon_F) \ll U + \epsilon_d, -\epsilon_d \ll D$.

The data symbols in Fig. 5(a) show T_K to be only weakly affected by Rashba coupling, just as was found in Ref. 15. The Kondo scale displays a quasi-linear ϵ_R dependence[34] with a slope that is positive for $\epsilon_d < -U/2$, negative for $\epsilon_d > -U/2$, and essentially vanishing for $\epsilon_d = -U/2$ (also in agreement with Ref. 15). Since the effective density of states $\rho(\epsilon)$ is independent of ϵ_R in a window of energies around ϵ_F, any modification of T_K must arise from changes in the total density of states near the band edges.

One can attempt to analyze the effect of density of states changes via a perturbative treatment along the lines of Haldane's derivation of poor-man's scaling equations for the Anderson impurity model[35]. This treatment, described further in Appendix A, can be used to map the Anderson impurity model with density of states $\rho(\epsilon)$ onto another Anderson impurity model with the no-Rashba density of states $\rho_0(\epsilon)$, but with the impurity parameters ϵ_d and U replaced by modified values $\tilde{\epsilon}_d$ and $\tilde{U}$ chosen so as to preserve (approximately) the same low-energy impurity properties as the original model. As explained in Appendix A, the hybridization matrix element V remains unchanged under this approach.

For purely quadratic band dispersion in the absence of Rashba SO interaction, expressions for the renormalized
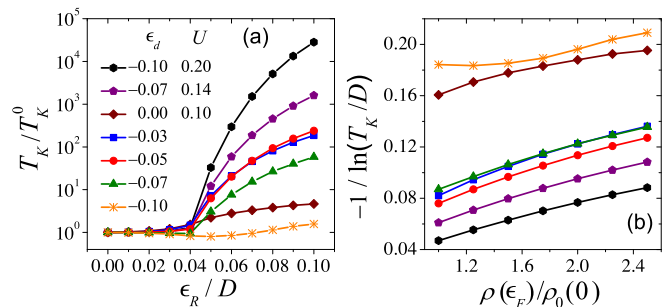

FIG. 6. (Color online) Kondo temperature for a constant band filling fraction $\eta \simeq 0.074$: (a) T_K/T_K^0 vs ϵ_R for different values of ϵ_d and U expressed in the legend in units of D; (b) results for $\epsilon_R \geq 0.04D$ plotted as $-1/\ln(T_K/D)$ vs $\rho[\epsilon_F(\epsilon_R)]/\rho_0(0)$. Data are for $\epsilon_0 = -0.08D$ and $\Gamma = 0.005D$.

parameter $\tilde{\epsilon}_d$ and $\tilde{U}$ can be obtained in closed form, but they are too cumbersome to reproduce here. Instead, Fig. 5(b) shows the evolution with ϵ_R of the shifts $\tilde{\epsilon}_d - \epsilon_d$ and $\tilde{U} - U$ for each of the three ϵ_d values illustrated in Fig. 5(a). An upward shift in the level energy and a downward shift in the on-site interaction both grow with ϵ_R and with $-\epsilon_d$, becoming 10% corrections in the most extreme case shown. Upon substitution into the Haldane formula [Eq. (45)], these shifts in $\tilde{\epsilon}_d$ and $\tilde{U}$ have opposite effects on T_K, so any overall change in T_K is the result of a subtle balance. The predicted curves for T_K/T_K^0 vs ϵ_R [solid lines in Fig. 5(a)] display the correct trends with growing $-\epsilon_d$, but the fact that NRG and perturbative curves for the same value of ϵ_d are not in close correspondence is an indication of the delicacy of the interplay between the parameter renormalizations.

Figure 6(a) shows very different behavior in cases where the band filling is fixed. For weak SO interaction, the total density of states $\rho(\epsilon)$ near the Fermi energy remains independent of ϵ_R, and T_K has a quasi-linear behavior similar to that found for fixed ϵ_F. However, once $\epsilon_R > |\epsilon_0|/2$, the system enters the helical metal regime and both $\rho(\epsilon_F)$ and $\Gamma(\epsilon_F)$ rise rapidly. This rise is magnified in the Kondo temperature due to the exponential dependence of T_K on $\Gamma(\epsilon_F)$ shown in Eq. (45). Figure 6(b) confirms such a dependence of the numerically determined value of T_K. The five lower curves exemplify the Kondo regime, where the weak deviations from linearity in this plot of $-1/\ln(T_K/D)$ vs $\rho(\epsilon_F)$ can be attributed primarily to the $\sqrt{\rho(\epsilon_F)}$ prefactor in Eq. (45). The remaining two cases ($U = 0.1D$, $\epsilon_d = 0$ and $\epsilon_d = -0.1D$) correspond to mixed valence, where the low-temperature scale is no longer expected to depend exponentially on $\Gamma(\epsilon_F)$.

3. Static angular-momentum correlations

Further insight can be gained into the nature of Kondo physics in presence of Rashba SO interaction by studying
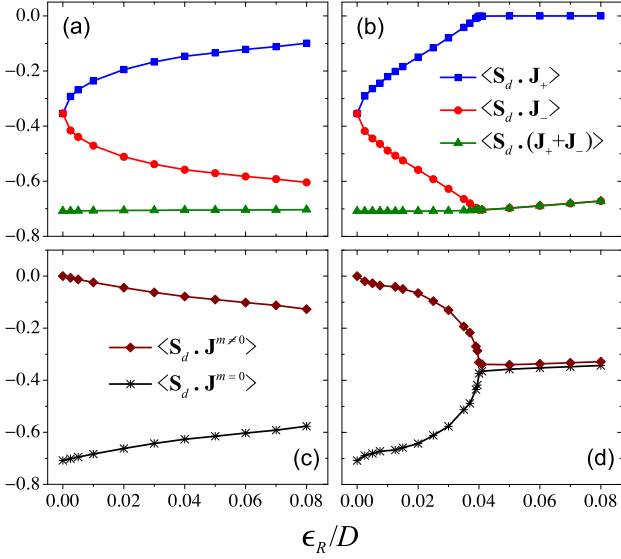
FIG. 7. (Color online) Static correlations between the impurity spin and the total angular momentum in different conduction-band channels, calculated for (a,c) fixed Fermi energy $\epsilon_R = 0$, or (b,d) constant band filling $\eta \approx 0.074$. The upper panels show $\langle \mathbf{S}_d \cdot \mathbf{J}_h \rangle$ for helicity $h = \pm$, while the lower panels plot the correlation of $\mathbf{S}_d$ with $\mathbf{J}^{m=0}$ (the total angular momentum of all electrons with orbital angular momentum $m = 0$) and with $\mathbf{J}^{m \neq 0}$ defined in Eq. (49). Data are for $\epsilon_0 = -0.08D$, $U = -2\epsilon_d = 0.1D$, and $\Gamma = 0.005D$.

the correlations between the impurity spin

$$\mathbf{S}_d = \tfrac{1}{2} \sum_{\tau, \tau'} d_\tau^\dagger \, \boldsymbol{\sigma}_{\tau, \tau'} \, d_{\tau'} \qquad (46)$$

and the total angular momentum

$$\mathbf{J}_h = \tfrac{1}{2} \sum_{\tau, \tau'} \int dk \, \tilde{c}_{k,h,\tau}^\dagger \, \boldsymbol{\sigma}_{\tau, \tau'} \, \tilde{c}_{k,h',\tau'} \qquad (47)$$

of all conduction-band electrons that have helicity h and angular momentum z component $\pm \tfrac{1}{2}$. The appendix provides details of how such correlations can be obtained within the NRG treatment of the two-channel Anderson Hamiltonian [Eq. 21]. The results presented below are static values calculated in the limit of absolute temperatures $T \to 0$.

Figure 7(a) plots $\langle \mathbf{S}_d \cdot \mathbf{J}_h \rangle$ vs ϵ_R under the scenario where the Fermi energy is fixed at $\epsilon_F = 0$. At zero Rashba energy, $\langle \mathbf{S}_d \cdot \mathbf{J}_h \rangle$ is the same for helicities $h = \pm$. As ϵ_R increases, the impurity spin becomes more strongly correlated with the $h = -$ channel and less strongly with the $h = +$ electrons. This can be understood as a density of states effect because the dimensionless ratio

$$r_h = \langle \mathbf{S}_d \cdot \mathbf{J}_h \rangle / [D \rho_h(\epsilon_F)] \qquad (48)$$

(not plotted) turns out to be almost independent of ϵ_R and h. Since the combined Fermi-level density of states $\rho(\epsilon_F) = \rho_+(\epsilon_F) + \rho_-(\epsilon_F)$ remains constant, it is therefore

unsurprising that $\langle \mathbf{S}_d \cdot (\mathbf{J}_+ + \mathbf{J}_-) \rangle$ barely changes with ϵ_R.

In cases where the band filling is constant [e.g., Fig. 7(b)], the behavior found for Rashba energies $\epsilon_R < -\epsilon_0/2$ is qualitatively the same as for fixed ϵ_F. However, once the helical regime is reached ($\epsilon_R > -\epsilon_0/2$), $\rho_+(\epsilon_F) = 0$ and $\langle \mathbf{S}_d \cdot \mathbf{J}_+ \rangle$ almost vanishes; the impurity spin is almost exclusively correlated with the $h = -$ channel. In this parameter range, the growth of $\rho_-(\epsilon_F)$ inside the helical regime increases the occupancy of the empty and doubly occupied impurity states and decreases the local-moment character, leading to a gradual decline in the magnitude of $\langle \mathbf{S}_d \cdot (\mathbf{J}_+ + \mathbf{J}_-) \rangle$ with increasing ϵ_R. The contrast with the fixed-ϵ_F scenario is highlighted by the facts that $r_+ = \infty$ due to the numerator on the right-hand side of Eq. (48) being small but nonzero due to correlation of $\mathbf{S}_d$ with high-energy electrons, while r_- rapidly approaches zero with increasing ϵ_R due to $\langle \mathbf{S}_d \cdot \mathbf{J}_- \rangle$ being nearly saturated but $\rho_-(\epsilon_F)$ still rising.

Figures 7(c) and 7(d) separate (for the fixed-ϵ_F and constant-η scenarios, respectively) two contributions to the overall impurity-band angular momentum correlation $\langle \mathbf{S}_d \cdot (\mathbf{J}_+ + \mathbf{J}_-) \rangle$: (i) $\langle \mathbf{S}_d \cdot \mathbf{J}^{m=0} \rangle$, where $\mathbf{J}^{m=0}$ is the total angular momentum of all electrons with orbital angular momentum $m = 0$, and (ii) $\langle \mathbf{S}_d \cdot \mathbf{J}^{m \neq 0} \rangle$, where

$$\mathbf{J}^{m \neq 0} = \mathbf{J}_+ + \mathbf{J}_- - \mathbf{J}^{m=0}. \qquad (49)$$

In both panels, the most striking result is the appearance for $\epsilon_R > 0$ of a nonzero correlation $\langle \mathbf{S}_d \cdot \mathbf{J}^{m \neq 0} \rangle$ that arises, not through direct interaction with the impurity (which is confined to $m = 0$), but rather indirectly through Rashba mixing of $m = 0$ states with $m = \pm 1$ states.

The details of Figs. 7(c) and 7(d) can be understood in terms of the helicity-resolved densities of states. Equation (11) shows that the operators $\tilde{c}_{k,h,\tau}$ entering Eq. (14) contain $m = 0$ and $m = \pm 1$ components of equal magnitude with a relative phase that is opposite for $h = +$ and $h = -$. For $\epsilon_R = 0$, the two helicity channels participate equally in Kondo screening in a manner that produces complete destructive interference of correlations contributing to $\langle \mathbf{S}_d \cdot \mathbf{J}^{m \neq 0} \rangle$. With increasing ϵ_R there is a growing difference $\rho_-(\epsilon) - \rho_+(\epsilon)$ for energies ϵ near ϵ_F, leading to imperfect cancellation of correlations between the impurity and $m = \pm 1$ electrons and a gradual convergence of $\langle \mathbf{S}_d \cdot \mathbf{J}^{m=0} \rangle$ and $\langle \mathbf{S}_d \cdot \mathbf{J}^{m \neq 0} \rangle$. Once the system enters the helical regime [$\epsilon_R > -\epsilon_0/2 = 0.04D$ in Fig. 7(d)], $\rho_+(\epsilon_F) = 0$, and the two correlation measures differ only due to contributions from electrons far from the Fermi energy.

B. Results with a Zeeman field

In order to study the combined effect of Rashba and Zeeman couplings on Kondo correlations, we have calculated the zero-temperature impurity polarization $M_{\text{imp}} = \langle J_z \rangle - \langle J_z \rangle_0$, where J_z is the z component of the total system angular momentum, and $\langle \ldots \rangle$ and $\langle \ldots \rangle_0$ denote,
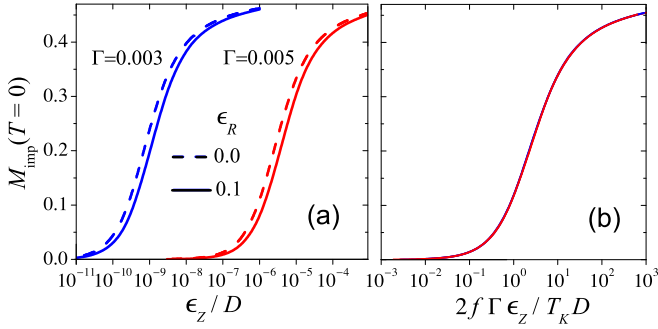
FIG. 8. (Color online) (a) Zero-temperature impurity polarization M_{imp} vs Zeeman energy ϵ_Z for $\epsilon_0 = -0.08D$, $U = -2\epsilon_d = 0.15D$, and for the values of Γ and ϵ_R labeled on the plot in units of D. (b) Same data as in (a), replotted vs $2f\Gamma\epsilon_Z/T_K D$, where $f = 2.4$ and 1.8 for $\epsilon_R/D = 0$ and 0.1, respectively.
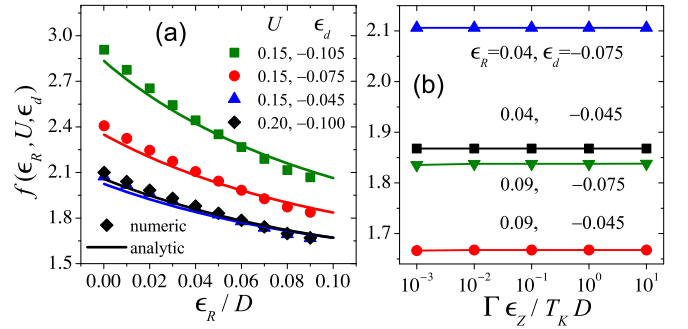

FIG. 9. (Color online). Quantity f entering the scaling collapse of the impurity polarization for a system with fixed Fermi energy $\epsilon_F = 0$: (a) f vs ϵ_R for different values of U and ϵ_d expressed in the legend in units of D. Each symbol was obtained via an NRG calculation of the compensating local field for $\Gamma\epsilon_Z/T_K D = 0.1$, while the lines represent algebraic results based on Eq. (50). (b) NRG values of f vs $\Gamma\epsilon_Z/T_K D$ for $U = 0.15D$ and different values of ϵ_R and ϵ_d expressed in the legend in units of D. Lines are guides to the eye showing that f is independent of ϵ_Z for $\Gamma\epsilon_Z/T_K D \lesssim 10$. Data in both panels are for $\epsilon_0 = -0.08D$ and $\Gamma = 0.005D$.

respectively, expectation values in the presence and absence of the impurity. M_{imp} is the natural extension of the usual impurity spin magnetization $\langle S_z \rangle - \langle S_z \rangle_0$, to which it reduces in the absence of Rashba coupling (i.e., for $\epsilon_R = 0$).

Initially, we focus on the scenario of fixed Fermi energy $\epsilon_F = 0$. Figure 8(a) shows the zero-temperature impurity polarization M_{imp} as a function of ϵ_Z for $U = -2\epsilon_d = 0.15D$, for $\epsilon_R/D = 0$ and 0.1, and for $\Gamma/D = 0.003$ and 0.005. The impurity parameters are such that for $\epsilon_R = 0$, the Kondo temperatures $T_K^0(\Gamma = 0.003D) \approx 4.4 \times 10^{-12}D$ and $T_K^0(\Gamma = 0.005D) \approx 2.6 \times 10^{-8}D$ differ by four orders of magnitude. As expected, M_{imp} is in all cases an increasing function of ϵ_Z. For a given value of $\epsilon_Z > 0$, M_{imp} is a decreasing function of ϵ_R. This can be understood by noting that the Zeeman field enters Eq. (43) in the combination $\epsilon_R - \tau\epsilon_Z$. Therefore, the splitting of the density of states for $\tau = \pm\frac{1}{2}$ becomes less significant with increasing Rashba coupling.

Figure 8(b) demonstrates a very good collapse of the polarization data in Fig. 8(a) when plotted as a function of $2f\Gamma\epsilon_Z/T_K D$, where T_K is the Kondo temperature for $\epsilon_Z = 0$ and f is a dimensionless fitting parameter that depends on ϵ_R. It is particularly notable that for given ϵ_R (including the case of no Rashba coupling), the Zeeman field is scaled by T_K/Γ rather than by the Kondo temperature itself, as would be the case for a nonzero impurity g factor. Small deviations from the scaling collapse occur only in the parameter range $\epsilon_Z \gtrsim \Gamma$.

The scaling shown in Fig. 8(b) can be understood via a second application of the perturbative treatment outlined in Appendix A. One can regard the Zeeman field as introducing a spin-dependent change $\Delta\rho_\tau = \rho_\tau(\epsilon) - \rho(\epsilon)$ in the density of states of electrons with angular momentum z component τ, where $\rho(\epsilon) = \rho_+(\epsilon) + \rho_-(\epsilon)$ is derived from Eq. (38). The perturbative method maps the problem to a one-channel Hamiltonian of the form of Eq. (24) in which both spin species share the same density of states $\rho(\epsilon)$ and to lowest order in ϵ_Z and Γ,

the on-site Coulomb repulsion U and the hybridization width Γ remain unchanged, but the impurity level energy becomes τ dependent[36]:

$$\tilde{\epsilon}_{d,\tau} \simeq \epsilon_d - 2\tau f(\epsilon_R, U, \epsilon_d)\,\Gamma\epsilon_Z/D. \qquad (50)$$

In other words, the Zeeman coupling effectively spin-splits the impurity level by an amount proportional to $\Gamma\epsilon_Z$. Just as would be the case if this splitting were caused by a magnetic field that coupled directly to the impurity spin, the Kondo correlations are destroyed when the splitting becomes comparable to T_K. In the present context, the result is a scaling dependence on the dimensionless quantity $\Gamma\epsilon_Z/DT_K$ rather than the conventional (i.e., $g_i \neq 0$) combination ϵ_Z/T_K. This conclusion is not restricted to situations involving Rashba SO interaction, and holds quite generally for realizations of the Anderson impurity model with $g_i = 0$.

Equation (A5) yields an algebraic expression for f to lowest order in ϵ_Z/ϵ_R that is rather cumbersome and will not be reproduced here. More generally, one can consider a combination of a bulk Zeeman splitting and a local field B_{loc} that couples only to the impurity. After integrating out the Zeeman field, one arrives at a renormalized impurity energy $\tilde{\epsilon}_{d,\tau} = \epsilon_d - 2\tau f(\epsilon_R, U, \epsilon_d)\,\Gamma\epsilon_Z/D + \tau g_i B_{\mathrm{loc}}$. This allows the numerical determination of f as $f = g_i B_{\mathrm{comp}}/(2\Gamma\epsilon_Z)$, where B_{comp} is the compensation value of the local field such that $\tilde{\epsilon}_{d,\tau} = \epsilon_d$ and hence $M_{\mathrm{imp}} = 0$.

Figure 9(a) illustrates the behavior of f vs ϵ_R for different combinations of U and ϵ_d. All cases show a monotonic decrease of f with increasing ϵ_R. There is also an interplay between U and ϵ_d, such that the f values for $(U/D, \epsilon_d/D) = (0.2, -0.1)$ and $(0.15, -0.045)$ lie almost on top of each other. In all the cases shown, there is good quantitative agreement between the numerical and
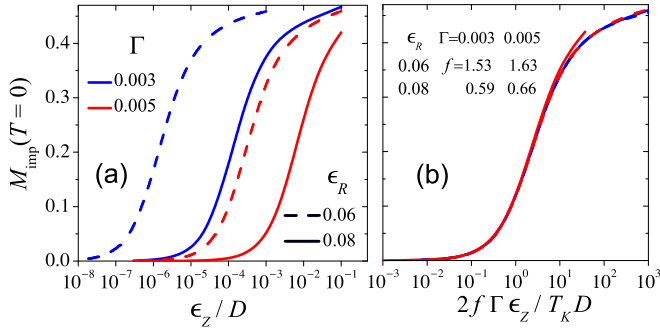
FIG. 10. (Color online) (a) Zero-temperature impurity polarization $M_{\rm imp}$ vs Zeeman energy ϵ_Z for $\epsilon_0 = -0.08D$, $U = -2\,\epsilon_d = 0.15D$, and for the values of Γ and ϵ_R labeled on the plot in units of D. (b) Same data as in (a), replotted vs $2f\Gamma\epsilon_Z/T_K D$ with values of f shown in the legend. In this case, f depends on Γ as well as ϵ_R.
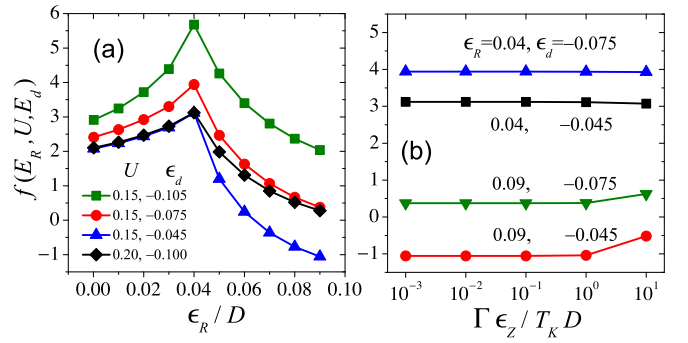

FIG. 11. (Color online) Quantity f entering the scaling collapse of the impurity polarization for a system with constant band filling $\eta \simeq 0.074$: (a) f vs ϵ_R for different values of U and ϵ_d expressed in the legend in units of D. Each symbol was obtained via an NRG calculation of the compensating local field for $\Gamma\epsilon_Z/T_K D = 0.1$, while the lines are guides to the eye. (b) NRG values of f vs $\Gamma\epsilon_Z/T_K D$ for $U = 0.15D$ and different values of ϵ_R and ϵ_d expressed in the legend in units of D. Line are guides to the eye showing that f is independent of ϵ_Z for $\Gamma\epsilon_Z/T_K D \lesssim 10$. Data in both panels are for $\epsilon_0 = -0.08D$ and $\Gamma = 0.005D$.

algebraic values plotted using symbols and lines, respectively.

Figure 9(b) shows f as a function of $\Gamma\epsilon_Z/T_K D$ for $U = 0.15D$ and a few selected values of ϵ_R and ϵ_d. The most salient feature is that f remains constant as $\Gamma\epsilon_Z/T_K D$ is varied over four orders of magnitude, indicating the lack of dependence on Γ and/or ϵ_Z. Deviations from universality are again seen only in the regime of very large Zeeman fields where the impurity polarization approaches saturation at $M_{\rm imp} = 0.5$.

Finally, we consider the effect of Zeeman splitting under the scenario of constant band filling. Figure 10(a) shows $M_{\rm imp}$ vs ϵ_Z for $U = -2\,\epsilon_d = 0.15D$, for $\epsilon_R/D = 0.06$ and 0.08, and for $\Gamma/D = 0.003$ and 0.005. Since Rashba SO interaction changes the Fermi-energy density of states, the Zeeman energy needed to destroy Kondo correlations is exponentially sensitive to both ϵ_R and Γ. As under the fixed-ϵ_F scenario, all the polarization curves share a similar shape (except for $\epsilon_Z \gtrsim \Gamma$) and a universal scaling dependence on $2f\Gamma\epsilon_Z/T_K D$ is confirmed in Fig. 10(b). In this case, however, the parameter f depends not just on ϵ_R, U, and ϵ_d, but also decreases with Γ. Under the constant-filling scenario, the Fermi level lies in an energy range where the density of states is spin-split, so a perturbative approach to first order in Γ is likely insufficient to reproduce the parameter dependences of f. For this reason, we focus on the numerical estimation of f via the compensation field. Figure 11 plots the results for the same parameters as were used in Fig. 9. Note that f exhibits a nonmonotonic dependence on ϵ_R, with a maximum at $\epsilon_R = -\epsilon_0/2 = 0.04D$. For $\epsilon_R \leq -\epsilon_0/2$, the value of f under the constant-filling scenario is generally greater than for fixed Fermi energy. For $\epsilon_R > -\epsilon_0/2$, the range where the system is in its helical regime for $\epsilon_Z = 0$, f decreases rapidly with increasing Rashba coupling and may even become negative.

IV. SUMMARY

We have studied the effect of bulk Rashba SO interaction on Kondo correlations between a magnetic impurity and a two-dimensional electron gas. The low-temperature thermodynamic properties exhibit the conventional Kondo form with scaling in terms of T/T_K, providing evidence for complete quenching of the impurity degree of freedom as $T \to 0$. In most situations, the Kondo temperature T_K is little affected by the Rashba coupling, as has been pointed out previously[15]. However, within a helical regime that can in principle be accessed for high Rashba couplings and/or low electron densities, the Kondo temperature exhibits an exponential enhancement compared to the situation without Rashba interaction.

Our analysis of static angular-momentum correlations demonstrates and quantifies an indirect, Rashba-induced coupling of the impurity spin with conduction channels of nonzero orbital angular momentum about the impurity site. This coupling can be regarded as a manifestation of a Dzyaloshinskii-Moriya term found previously by mapping the Anderson impurity model with bulk Rashba SO interaction to an effective Kondo model[18]. A perturbative renormalization-group analysis of this Kondo model showed an exponential enhancement of T_K. We should note, however, that the RG equations were solved neglecting the helicity dependence of the Fermi wave vector. A complete analysis of the effective Kondo model will be presented elsewhere.

Optical irradiation experiments seem to be good candidates to explore the helical regime of a Rashba-coupled 2DEG. Motivated by the proposal of Ref. 21, we have also investigated Kondo physics in the presence of both

Rashba SO interaction and Zeeman splitting of the bulk electrons (but not of the impurity). The characteristic Zeeman energy scale for the destruction of the Kondo effect is not T_K, as would be expected in the case of a true magnetic field that couples directly to the impurity spin, but rather T_K/Γ where Γ is the impurity hybridization width. The behavior can be accounted for to reasonable quantitative accuracy by a perturbative treatment of the Zeeman splitting of the host density of states.

Appendix A: Perturbative Analysis

This appendix considers an Anderson impurity model

$$
H = \sum_\sigma \int d\epsilon\, \epsilon\, c^\dagger_{\epsilon,\sigma} c_{\epsilon,\sigma} + \sum_\sigma \epsilon_{d,\sigma} d^\dagger_\sigma d_\sigma + U d^\dagger_\uparrow d_\uparrow d^\dagger_\downarrow d_\downarrow
$$
$$
+ \sum_\sigma V_\sigma \int d\epsilon\, \rho_\sigma(\epsilon) \left(c^\dagger_{\epsilon,\sigma} d_\sigma + \text{H.c.} \right), \quad \text{(A1)}
$$

where the conduction-band density of states $\rho_\sigma(\epsilon)$, the impurity level energy $\epsilon_{d,\sigma}$, and the hybridization matrix element V_σ are all allowed to depend on $\sigma = \uparrow, \downarrow$. The goal is to construct an approximate mapping of Eq. (A1) to a similar Hamiltonian having a different conduction-band density of states $\tilde{\rho}_\sigma(\epsilon)$, and with the impurity parameters $\tilde{\epsilon}_{d,\sigma}$, $\tilde{U}$, and $\tilde{V}_\sigma$ chosen to ensure that the two models share the low-energy physics (at least as it pertains to the impurity properties).

Haldane, in his derivation of poor-man's scaling equations for the Anderson model[35], used perturbation theory in the hybridization matrix element to take into account the effect of all conduction-band states in a narrow window of energies near each band edge. Here, we perform a similar calculation in order to find energy shifts arising from the density-of-states difference $\Delta\rho_\sigma(\epsilon) = \rho_\sigma(\epsilon) - \tilde{\rho}_\sigma(\epsilon)$ at all energies ϵ. Like Haldane, our focus is on four many-body states $|0\rangle$, $|\sigma\rangle = d^\dagger_\sigma |0\rangle$, and $|2\rangle = d^\dagger_\uparrow d^\dagger_\downarrow |0\rangle$, formed by combining the conduction-band ground state [having N_k electrons of energy $\epsilon(\mathbf{k}) < \epsilon_F$] with one of the possible configurations of the Anderson impurity level. These many-body states have energies E_0, $E_\sigma = E_0 + \epsilon_d$, and $E_2 = E_\uparrow + E_\downarrow - E_0 + U$, respectively.

The state $|0\rangle$ can decrease its energy through virtual tunneling of an electron of spin σ from a band state below

the Fermi level to the impurity and then back to the original band state. Integrating the contribution to such processes arising just from the density of states difference $\Delta\rho_\sigma(\epsilon)$, then summing over σ, transforms the state $|0\rangle$ to one $|\tilde{0}\rangle$ having an energy $\tilde{E}_0$ that, to second order in V, is

$$
\tilde{E}_0 = E_0 - \sum_\sigma V_\sigma^2 \int_{-\infty}^{\epsilon_F} \frac{\Delta\rho_\sigma(\epsilon)\, d\epsilon}{-\epsilon + \epsilon_{d,\sigma}}. \quad \text{(A2)}
$$

Similarly, the state $|2\rangle$ can decrease its energy through virtual tunneling of a spin-σ electron from the impurity to a band state above the Fermi level and then back to the impurity. The contribution to such processes arising from $\Delta\rho_\sigma(\epsilon)$, when summed over σ, transforms $|2\rangle$ to $|\tilde{2}\rangle$ with energy

$$
\tilde{E}_2 = E_2 - \sum_\sigma V_\sigma^2 \int_{\epsilon_F}^{\infty} \frac{\Delta\rho_\sigma(\epsilon)\, d\epsilon}{\epsilon - U - \epsilon_{d,\sigma}}. \quad \text{(A3)}
$$

Lastly, the state $|\sigma\rangle$ can lower its energy through (i) tunneling of an electron with spin σ from the impurity to a band state above the Fermi level and then back to the impurity, and (ii) tunneling of an electron with spin $-\sigma$ from a band state below the Fermi energy to the impurity and then back to the original band state. The contribution to such processes arising from $\Delta\rho(\epsilon)$ transforms $|\sigma\rangle$ to $|\tilde{\sigma}\rangle$ with energy

$$
\tilde{E}_\sigma = E_\sigma - V_\sigma^2 \int_{\epsilon_F}^{\infty} \frac{\Delta\rho_\sigma(\epsilon)\, d\epsilon}{\epsilon - \epsilon_{d,\sigma}} - V_{-\sigma}^2 \int_{-\infty}^{\epsilon_F} \frac{\Delta\rho_{-\sigma}(\epsilon)\, d\epsilon}{-\epsilon + U + \epsilon_{d,-\sigma}}. \quad \text{(A4)}
$$

Equations (A2)–(A4) can be used to define shifted impurity parameters

$$
\tilde{\epsilon}_{d,\sigma} = \tilde{E}_\sigma - \tilde{E}_0 \quad \text{(A5)}
$$

and

$$
\tilde{U} = \tilde{E}_2 + \tilde{E}_0 - \tilde{E}_\uparrow - \tilde{E}_\downarrow. \quad \text{(A6)}
$$

Corrections to the hybridization matrix elements (arising as a consequence of wave-function renormalization) are found to be of order V^3, so at the level of our approximation,

$$
\tilde{V}_\sigma = V_\sigma. \quad \text{(A7)}
$$

Since $\Delta\rho_\sigma(\epsilon)$ everywhere enters the above equations multiplied by V_σ^2, the analysis can be recast as the derivation of shifts in the impurity parameters ϵ_d and U to account for a change $\Delta\Gamma_\sigma(\epsilon) = \pi\, \Delta\rho_\sigma(\epsilon)\, V_\sigma^2$ in the spin-dependent hybridization function.

We note that an equation equivalent to Eq. (A4) appears in Refs. 37 and 38, which examine the spin splitting of the impurity level arising from entirely integrating out the conduction band. In our language, this case corresponds to $\tilde{\rho}_\sigma(\epsilon) = 0$ and $\Delta\rho_\sigma(\epsilon) = \rho_\sigma(\epsilon)$. These earlier works did not take into account changes in the energies of the empty and doubly occupied states that can lead to a shift in the on-site interaction U.

Appendix B: Computation of Angular-Momentum Correlations

This appendix describes the calculation of static correlations between the impurity spin $\mathbf{S}_d$ defined in Eq. (46) and one of $\mathbf{J}_h$, $\mathbf{J}^{m=0}$, and $\mathbf{J}^{m\neq0}$ representing the total angular momentum operators of helicity-h electrons, of electrons having orbital angular momentum $m=0$, and of electrons with angular momentum $m\neq0$.

Within the numerical renormalization-group treatment of the effective two-channel Anderson model described by Eq. (21), an appropriate representation of $\mathbf{J}_h$ [defined in Eq. (47)] for the calculation of the thermal average $\langle\mathbf{S}_d\cdot\mathbf{J}_h\rangle$ at temperatures $T\sim D\Lambda^{-N/2}$ is

$$\mathbf{J}_h = \sum_{n=0}^{N}\mathbf{J}_{n,h} \tag{B1}$$

with

$$\mathbf{J}_{n,h} = \tfrac{1}{2}\sum_{\tau,\tau'}\tilde{f}_{n,h,\tau}^{\dagger}\,\boldsymbol{\sigma}_{\tau,\tau'}\,\tilde{f}_{n,h,\tau'}, \tag{B2}$$

where $\tilde{f}_{n,h,\tau}$ destroys an electron of total angular momentum z component $\tau=\pm1/2$ on site n of the Wilson chain that results[29] from applying the Lanczos procedure to a discretized version of the bulk Hamiltonian H_{bulk} in Eq. (12).

The calculation of $\langle\mathbf{S}_d\cdot\mathbf{J}^{m=0}\rangle$ and $\langle\mathbf{S}_d\cdot\mathbf{J}^{m\neq0}\rangle$, related to $\langle\mathbf{S}_d\cdot\mathbf{J}_h\rangle$ by Eq. (49), is more complicated since orbital angular momentum is not a good quantum number of the bulk states. Since the NRG Lanczos procedure preserves spin and orbital angular momenta, one can write

$$\tilde{f}_{n,h,\tau} = \frac{1}{\sqrt{2}}\big(h^{\tau-1/2}f_{n,\tau-1/2,\uparrow}+h^{\tau+1/2}f_{n,\tau+1/2,\downarrow}\big) \tag{B3}$$

in terms of annihilation operators $f_{n,m,\tau}$ for orbital angular momentum eigenstates, in direct analogy with Eq. (11). Substitution of Eq. (B3) into Eq. (B2) allows one to write

$$\mathbf{J}_{n,+}+\mathbf{J}_{n,-} = \mathbf{J}_n^{m=0}+\mathbf{J}_n^{m\neq0}, \tag{B4}$$

where

$$\mathbf{J}_n^{m=0} = \tfrac{1}{2}\sum_{\tau,\tau'}f_{n,0,\tau}^{\dagger}\,\boldsymbol{\sigma}_{\tau,\tau'}\,f_{n,0,\tau'}, \tag{B5}$$

$$\mathbf{J}_n^{m\neq0} = \tfrac{1}{2}\sum_{\tau,\tau'}f_{n,2\tau,-\tau}^{\dagger}\,\boldsymbol{\sigma}_{\tau,\tau'}\,f_{n,2\tau',-\tau'}, \tag{B6}$$

$$\tag{B7}$$

Equation (B6) makes clear that $\mathbf{J}_n^{m\neq0}$ includes terms that are off-diagonal in the orbital angular momentum index.

Equation (B3) can be inverted to yield, for $m=0$, $\tau=\pm\tfrac{1}{2}$ and for $m=\pm1$, $\tau=\mp\tfrac{1}{2}$,

$$f_{n,m,\tau} = \frac{1}{\sqrt{2}}\big[\tilde{f}_{n,+,\tau}+(-1)^m\tilde{f}_{n,-,\tau}\big]. \tag{B8}$$

Substitution of Eq. (B8) into Eqs. (B5) and (B6) yields

$$\mathbf{J}^{m=0} = \tfrac{1}{2}\sum_{n=0}^{N}\big(\mathbf{J}_{n,+}+\mathbf{J}_{n,-}+\tilde{\mathbf{J}}_n\big) \tag{B9}$$

$$\mathbf{J}^{m\neq0} = \tfrac{1}{2}\sum_{n=0}^{N}\big(\mathbf{J}_{n,+}+\mathbf{J}_{n,-}-\tilde{\mathbf{J}}_n\big), \tag{B10}$$

where

$$\tilde{\mathbf{J}}_n = \tfrac{1}{2}\sum_{h,\tau,\tau'}\tilde{f}_{n,h,\tau}^{\dagger}\,\boldsymbol{\sigma}_{\tau,\tau'}\,\tilde{f}_{n,-h,\tau'} \tag{B11}$$

is off-diagonal in the helicity index.

Equations (B1), (B2), and (B9)–(B11) contain the prescription for constructing the total angular momentum operators in our NRG calculations. In order to obtain ground-state correlations, we took the thermal averages of $\mathbf{S}_d$ with $\mathbf{J}_h$, $\mathbf{J}^{m=0}$, and $\mathbf{J}^{m\neq0}$ in the limit of large iteration numbers corresponding to temperature scales far below T_K.

* Present address: Centro de Nanociencas y Nanotecnología, Universidad Nacional Autónoma de México, Ensenada, Baja California, 22800, Mexico

[1] S. A. Wolf, D. D. Awschalom, R. A. Buhrman, J. M. Daughton, S. von Molnár, M. L. Roukes, A. Y. Chtchelkanova, and D. M. Treger, Science **294**, 1448 (2001).

[2] I. Žutić, J. Fabian, and S. Das Sarma, Rev. Mod. Phys. **76**, 323 (2004).

[3] R. Winkler, *Spin-orbit coupling effects in two-dimensional electron and hole systems* (Springer-Verlag, Berlin, 2003).

[4] T. Jungwirth, J. Sinova, J. Mašek, J. Kucera, and A. H. MacDonald, Rev. Mod. Phys. **78**, 809 (2004).

[5] T. Jungwirth, J. Wunderlich, and K. Olejník, Nat. Materials **11**, 382 (2012).

[6] P. D. C. King *et al.*, Phys. Rev. Lett. **107**, 096802 (2011).

[7] Z.-H. Zhu *et al.*, Phys. Rev. Lett. **107**, 186405 (2011).

[8] D. Gainon and A. J. Heeger, Phys. Rev. Lett. **22**, 1420 (1969).

[9] B. Giovannini, Phys. Rev. B **3**, 870 (1971).

[10] H. U. Everts, Z. Phys. **251**, 42 (1972).

[11] G. Bergmann, Phys. Rev. Lett. **57**, 1460 (1986).

[12] Y. Meir and N. S. Wingreen, Phys. Rev. B **50**, 4947 (1994).

[13] E. Eriksson, A. Ström, G. Sharma, and H. Johannesson, Phys. Rev. B **86**, 161103(R) (2012).

[14] J. Malecki, J. Stat. Phys. **129**, 741 (2007).

[15] R. Žitko and J. Bonča, Phys. Rev. B **84**, 193411 (2011).

[16] L. Isaev, D. F. Agterberg, and I. Vekhter, Phys. Rev. B **85**, 081107(R) (2012).

[17] J. R. Schrieffer and P. A. Wolff, Phys. Rev. **149**, 491 (1966).

[18] M. Zarea, S. E. Ulloa and N. Sandler, Phys. Rev. Lett. **108**, 046601 (2012).

[19] D. Mastrogiuseppe, A. Wong, K. Ingersent, S. E. Ulloa, and N Sandler, Phys. Rev. B **90**, 035426 (2014).

[20] For example, see J. Huang, L. N. Pfeiffer, and K. W. West, Phys. Rev. Lett. **112**, 036803 (2014).

[21] T. Ojanen and T. Kitagawa, Phys. Rev. B **85**, 161202(R) (2012).

[22] N. H. Lindner, G. Refael, and V. Galitski, Nat. Phys. **7**, 490 (2011).

[23] B. Dóra, J. Cayssol, F. Simon, and R. Moessner, Phys. Rev. Lett. **108**, 056602 (2012).

[24] P. B. Vigman and A. M. Finkel'shtein, Sov. Phys. JETP **48**, 102 (1978).

[25] N. Andrei, K. Furuya and J. H. Lowenstein, Rev. Mod. Phys. **55**, 331 (1983).

[26] Throughout this paper, we work in units where $\hbar = k_B = g_b \mu_B = 1$.

[27] G. Allison, T. Fujita, K. Morimoto, S. Teraoka, M. Larsson, H. Kiyama, A. Oiwa, S. Haffouz, D. G. Austing, A. Ludwig, A. D. Wieck, and S. Tarucha, Phys. Rev. B **90**, 235310 (2014).

[28] We have displaced the angular argument ϕ_k by $\pi/2$ to absorb the prefactor of i in H_{Rashba} as defined in Eq. (3).

[29] H. R. Krishna-murthy, J. W. Wilkins, and K. G. Wilson, Phys. Rev. B **21**, 1003 (1980).

[30] R. Bulla, T. Pruschke, and A. C. Hewson, J. Phys.: Condens. Matt. **9**, 10 463 (1997).

[31] C. Gonzalez-Buxton and K. Ingersent Phys. Rev. B **57**, 14 254 (1998).

[32] W. C. Oliveira and L. N. Oliveira, Phys. Rev. B **49**, 11986 (1994).

[33] F. D. M. Haldane, J. Phys. C **11**, 5015 (1978).

[34] Quasi-linear variation of T_K with ϵ_R has been reported previously for within two-impurity Anderson model: T. I. Ivanov, Phys. Rev. B **86**, 155429 (2012).

[35] F. D. M. Haldane, Phys. Rev. Lett. **40** 416, 911(E) (1987).

[36] A field-induced splitting of the level energy of an Anderson impurity has been calculated via a similar perturbative calculation in the context of quantum dots connected to ferromagnetic leads; see Refs. 37 and 38, as well as Ref. 39 for a related experiment.

[37] J. Martinek, M. Sindel, L. Borda, J. Barnás, R. Bulla, J. König, G. Schön, S. Maekawa, and J. von Delft, Phys. Rev. B **72**, 121302(R) (2005).

[38] M. Sindel, L. Borda, J. Martinek, R. Bulla, J. König, G. Schön, S. Maekawa, and J. von Delft, Phys. Rev. B **76**, 045321 (2007).

[39] J. R. Hauptmann, J. Paaske, and P. E. Lindelof, Nature Phys. **4**, 373 (2008).